

Incorporating Exemplar Optimization into Training with Dual Networks for Human Mesh Recovery

Yongwei Nie¹, Mingxian Fan¹, Chengjiang Long², Qing Zhang³, Jian Zhu⁴, Xuemiao Xu¹

¹South China University of Technology, China ²Meta Reality Labs, USA

³Sun Yat-sen University, China ⁴Guangdong University of Technology, China

nieyongwei@scut.edu.cn

Abstract

We propose a novel optimization-based human mesh recovery method from a single image. Given a test exemplar, previous approaches optimize the pre-trained regression network to minimize the 2D re-projection loss, which however suffer from over-/under-fitting problems. This is because the “exemplar optimization” at testing time has too weak relation to the pre-training process, and the exemplar optimization loss function is different from the training loss function. (1) We incorporate exemplar optimization into the training stage. During training, our method first executes exemplar optimization and subsequently proceeds with training-time optimization. The exemplar optimization may run into a wrong direction, while the subsequent training optimization serves to correct the deviation. Involved in training, the exemplar optimization learns to adapt its behavior to training data, thereby acquires generalibility to test exemplars. (2) We devise a dual-network architecture to convey the novel training paradigm, which is composed of a main regression network and an auxiliary network, in which we can formulate the exemplar optimization loss function in the same form as the training loss function. This further enhances the compatibility between the exemplar and training optimizations. Experiments demonstrate that our exemplar optimization after the novel training scheme significantly outperforms state-of-the-art approaches.

1. Introduction

Human mesh recovery (HMR) from a single image is of great importance to many human-related applications, such as action capture without MoCap device, action transfer with vision-based system, and VR/AR entertainments, etc. This topic has received lots of research during past years. Most of existing approaches represent the 3D human mesh by a parametric human model such as SMPL [35], and the aim is to estimate the parameters $\Theta = (\theta, \beta)$, where θ encodes the



Figure 1. (a) EFT_{CLIFF} overfits wrong poses by OpenPose [6], where CLIFF [32] is the regressor fine-tuned by EFT [21]. Our method ignores wrong joints and fits the target human faithfully. (b) EFT_{CLIFF} is lost in local minima and cannot fit correct poses. Our method does not suffer from underfitting for the two cases.

pose of mesh, while β describes the body shape.

The existing single-image HMR methods can generally be categorized into two classes of regression-based approaches and optimization-based approaches. The regression approaches [8, 22, 32, 33, 52, 55, 56, 62] train a neural network to directly output a 3D SMPL mesh given an input image. Although regression approaches can learn powerful prior knowledge and produce nearly correct human meshes for most images, we still often observe small deviations between the projected hands and feet and the 2D evidences.

The optimization-based approaches of EFT [21] and BOA [15] alleviate this problem by performing a post-processing stage on any a test exemplar. They first extract 2D evidences from the test image (e.g., 2D pose), then further optimize the parameters of the pre-trained network to make the network overfit the 2D evidences. We refer to this as “*exemplar optimization*”. However, the exemplar optimization may be misled by *wrong* 2D poses (Figure 1 (a)), and sometimes still suffers from the underfitting problem (Figure 1 (b)).

In this paper, we propose a method to tackle the over-/under-fitting problems of exemplar optimization, and significantly improve the mesh recovery accuracy both quantitatively and qualitatively. Our method is based on two observations. First, currently, the exemplar optimization is independent of the pre-training process, only using the pre-trained parameters as the optimization starting point. Second, the exemplar optimization loss function is different from the training loss function due to lack of 3D supervision. Both factors make the parameter subspace around the pre-trained network not compatible with the exemplar optimization. Therefore, exemplar optimization in this space can easily get stuck in local minima (overfitting) or hit obstacles (underfitting).

Our solution is a novel dual-network training framework (see overview in Figure 2) that improves the current exemplar optimization methods from two aspects. First, to overcome the problem that current exemplar optimization is independent of the pre-training, we propose to incorporate the exemplar optimization into the training process, inspired by optimization-based meta learning [12]. Specifically, given a training sample, our method first performs exemplar optimization on this sample to update the regression network specific to the sample. Then, based on all pieces of regression networks after exemplar optimizations, we further optimize the training-time objective over the whole set of training exemplars. In this way, we achieve the goal of optimizing both exemplar and training objectives. By performing the overall training-time optimization after exemplar optimization, one can imagine that we actually use the overall optimization as a faithful supervision to correct the wrong optimization directions of the exemplar optimization. After the training, the regressor and the parameter space around regressor are optimal for the exemplar optimization, and accordingly our new exemplar optimization shows generalibility during testing.

Second, to overcome the problem that exemplar and training optimizations have different loss functions, we design a dual-network structure with a main regression network and an auxiliary network. The auxiliary network furnishes the main network with pseudo SMPL meshes, based on which we unify the formulations of exemplar and training optimization loss functions. This further enhances the compatibility between exemplar and training optimizations, and also avoids the exemplar optimization controlled by only 2D joints like in EFT [21].

At testing time, we freeze the auxiliary network’s parameters and conduct the exemplar optimization to the main network using the learned main regression parameters as the optimization starting point. We conduct extensive experiments on five training datasets and validation on two HMR benchmarks. The experiments suggest that our exemplar optimization after the novel dual-network training leads to superior HMR performance to the state-of-the-art approaches.

To summarize, our main contributions of this paper are three-fold:

- We propose a novel dual-network HMR framework with exemplar optimization involved into the joint-training procedure, which effectively alleviates the over-/under-fitting problem of previous exemplar optimization approaches.
- We ensure the exemplar optimization objective identical to the overall training objective, which further facilitates the joint-training and interaction between our well-designed dual networks.
- Experiments show that our results outperform those of previous approaches significantly in both quantitative and qualitative comparisons.

2. Related Work

We focus on methods utilizing a monocular image for 3D human mesh reconstruction and broadly categorize them into regression-based and optimization-based approaches. As our approach resembles model agnostic meta-learning [12], we also review relevant works in this field.

Regression-based methods. Regression-based methods typically employ deep neural networks to regress the human body mesh representation from images directly. In most cases, these methods [11, 22, 25, 38, 41, 42, 50, 54, 57, 60, 61] choose to regress parametric human body model, such as SMPL [35]. Early works such as HMR [22] employed CNN [17] to extract features and MLP layers to output 3D mesh parameters. Later, more sophisticated networks were considered for improving the reasoning accuracy. For example, PyMAF [60, 61] extracted features in a pyramid structure and iteratively aligned 3D vertices with human body in the image. Xue et al. [55] proposed using a learnable mask to automatically identify the most discriminative features related to 3D mesh recovery. In [26, 32, 52], it was observed that prior works often overlooked the importance of camera parameters. CLIFF [32] innovatively considered using the cropping bounding boxes as input to reduce the ambiguity in reprojection loss. Zolly [52] further considered the camera distortion produced by perspective projection.

There are also non-parameterized methods that directly regress mesh vertices. For example, METRO [33] utilized Transformer to model the global relationship between human keypoints and mesh vertices, which however had shortcomings in terms of parameter count and inference speed.

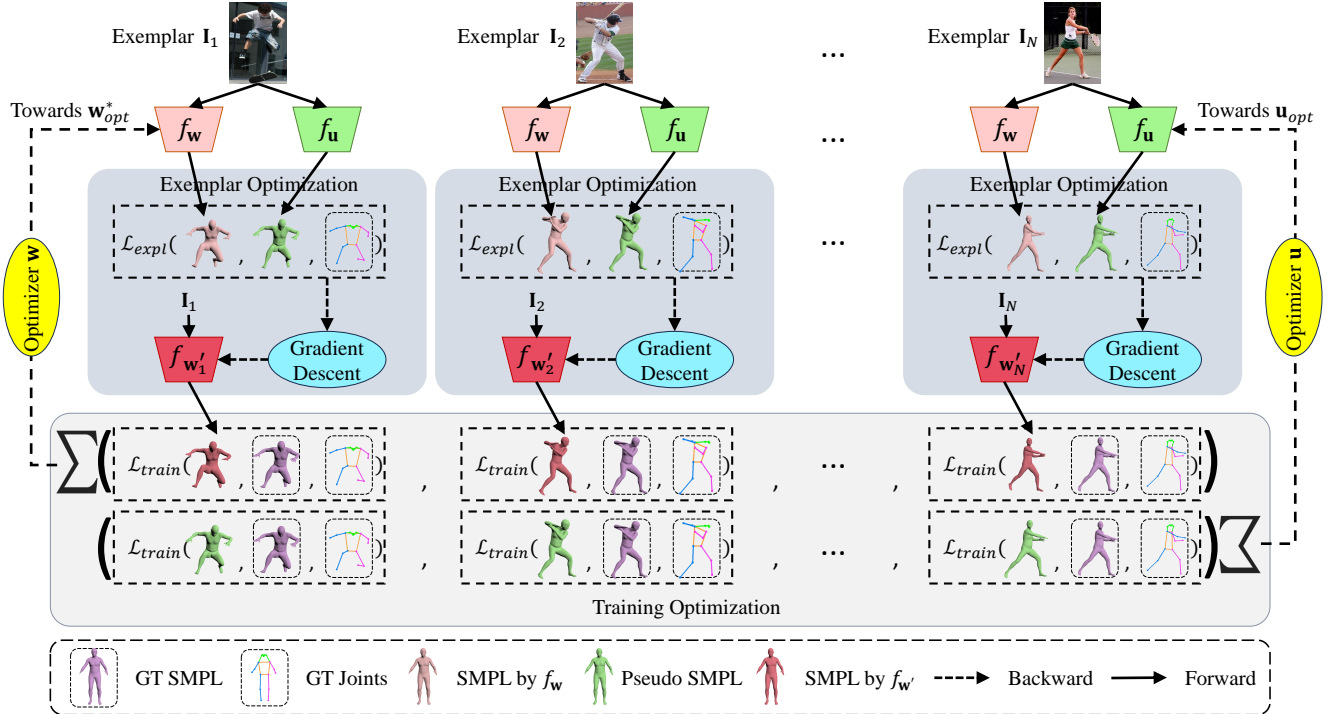


Figure 2. **Overview of our proposed dual-network framework.** It is composed of a main HMR regression network f_w and an auxiliary network f_u which share the same architecture (all training exemplars share the same f_w and f_u which are drawn separately for ease of illustration), and two optimization objectives \mathcal{L}_{expl} and \mathcal{L}_{train} . The exemplar optimization is executed for each exemplar I_i individually to update f_w to $f_{w'_i}$, by performing one gradient descent step to w according to the exemplar loss function \mathcal{L}_{expl} . Then, we execute the training loss function based on the networks updated by exemplar optimizations. One part of the training loss function is used to optimize the main regression network and the other part is to optimize the auxiliary network. After training, we obtain the optimal parameters w_{opt}^* and u_{opt}^* for the main and auxiliary networks respectively, as defined in the paper.

FastMETRO [8] addressed this by separating the backbone features from the features corresponding to keypoints and vertices. Recently, [56] combined pyramid structure in PyMAF [60, 61] with the Transformer-based HMR regression method, further improving the regression accuracy.

The regression model is a key component in our method. Theoretically, any end-to-end regression model can be upgraded by our method by incorporating exemplar optimization into their training process. Without loss of generality, we have tested HMR and CLIFF as the regression network in our method.

Optimization-based methods. Optimization-based methods [3, 5, 14, 16, 21, 29, 43, 46, 63] usually attempt to estimate a 3D body mesh consistent with 2D image cues. Bogo et. al. proposed an automatic approach called SMPLify [5], which iteratively adjusts SMPL parameters to fit the detected 2D keypoints. SPIN [27] combined regression-based methods with SMPLify, utilizing the regression results as initialization for SMPLify. Simultaneously, the optimization results from SMPLify provided supervision for the regressor. Similarly, CycleAdapt [39] alternately trains a HMR network and a motion denoising network to enhance each

other. Unlike SMPLify, EFT [21] and BOA [15] fine-tuned the pre-trained 3D mesh regression network via 2D reprojection loss or temporal consistency loss at test phase, rather than updating the SMPL parameters. In order to achieve a better fit for 3D mesh and mitigate the ambiguity of 2D observations, some approaches propose learning stronger 3D priors [10, 28, 39, 43] or utilizing trainable neural networks to update parameters in lieu of gradient updates [9, 47, 58]. Inverse kinematics (IK) has also been explored. Some methods address IK problems by decomposing relative rotations [30], designing networks that integrate forward and inverse kinematics [31], or incorporating UV position maps [45].

Different from all the above, the goal of this paper is to overcome the problem of exemplar optimization approaches [15, 21] that the optimization at testing time is disconnected with the optimization at training time, to make the exemplar optimization generalize better during testing.

Meta Learning. Our method is most related to the optimization based meta-learning MAML [12]. MAML first samples a number of tasks, then performs local optimization on each task, and finally conducts a global optimization to update the parameters of the original network. This is

very similar to our method that first executes exemplar optimization on each training exemplar and then performs training optimization on a batch of training samples. However, although our method is inspired by MAML and its extensions [2, 40, 44], our goal is fundamentally different from theirs. The goal of MAML is usually for few-shot learning or domain adaptation, which assumes there is ground-truth labeled data in the target domain. With MAML, the network can quickly adapt it to the new domain by learning on the few labeled data. In contrast, our goal is to adapt the network to a single test exemplar which is free of ground-truth human mesh. We have noted MAML has been proven effective in various domains, such as talking head generation [59], SVBRDF recovery [13, 64], 3D GAN inversion [19], etc. However, there is rare work applying meta learning for HMR, except the recent work [23] which however discards 3D ground-truth SMPL meshes during training.

3. Method

Our goal is to estimate a 3D SMPL human mesh parameterized by $\Theta = (\theta, \beta)$ together with a camera π from a given image \mathbf{I} of a person, where $\theta \in \mathbb{R}^{24 \times 3}$ and $\beta \in \mathbb{R}^{10}$ are pose and shape parameters of the SMPL human model [35], respectively.

Given a large dataset $\{\mathbf{I}_i, \hat{\Theta}_i, \hat{\mathbf{J}}_i\}_{i=1}^N$, where \mathbf{I}_i is a training image, $\hat{\Theta}_i$ is the ground-truth (GT) human mesh, $\hat{\mathbf{J}}_i$ is the 2D GT joints of the human in the input image, N is the size of training dataset, we can train a regression neural network $f_{\mathbf{w}} : \mathbf{I}_i \rightarrow (\Theta_i, \pi_i)$ by the following generalized regression formulation:

$$\mathbf{w}_{opt} = \arg \min_{\mathbf{w}} \sum_{i=1}^N \mathcal{L}_{train}(f_{\mathbf{w}}(\mathbf{I}_i), \hat{\Theta}_i, \hat{\mathbf{J}}_i), \quad (1)$$

where \mathcal{L}_{train} is the training loss consisting of 2D reprojection loss with respect to $\hat{\mathbf{J}}_i$ and 3D SMPL losses with respect to $\hat{\Theta}_i$ (see loss functions in Section 3.4).

The above regression method can learn powerful priors, but the priors are learned on the whole dataset and may not be applicable to every single test sample, because of which we often see misalignment between the projected human mesh and 2D person in the image, at testing time.

3.1. Preliminary: Exemplar Optimization

Exemplar-Fine-Tuning (EFT) [21] is first proposed as an exemplar optimization method to adjust the output of the network according to any specific test sample. After adjustment, the output of the network is enforced to match with the 2D evidences as closely as possible to compensate for the misalignment problem of the regression method.

In particular, at the testing stage, the pre-trained network \mathbf{w}_{opt} is further optimized on any a specific test image \mathbf{I}_i by

performing the following exemplar fine-tuning (EFT):

$$\mathbf{w}_i^* = \arg \min_{\mathbf{w}_i} \mathcal{L}_{expl}(f_{\mathbf{w}_i}(\mathbf{I}_i), \hat{\mathbf{J}}_i), \text{ starting from } \mathbf{w}_{opt}, \quad (2)$$

where again $\hat{\mathbf{J}}_i$ is the 2D GT human joints (usually detected by OpenPose [6]) in image \mathbf{I}_i and \mathcal{L}_{expl} is the exemplar optimization objective composed of 2D reprojection loss with respect to $\hat{\mathbf{J}}_i$ and some prior/regularization losses. Note that the initial \mathbf{w}_i in the above exemplar optimization is set to \mathbf{w}_{opt} , as the goal of this process is to fine-tune the pre-trained network.

It is worth mentioning here that the exemplar optimization in EFT is only applied at the testing stage, which heavily depends on the initial generalized regression model \mathbf{w}_{opt} , but \mathbf{w}_{opt} and the parameter space around \mathbf{w}_{opt} are not specially established for the objective of the postponed exemplar optimization. Accordingly, EFT may produce inferior results as shown in Figure 1 which demonstrate the model \mathbf{w}_{opt} is not well-adapted to these specific test samples.

3.2. Incorporating Exemplar Optimization into Training

The key observation of this paper is that in the work of EFT [21], the training optimization in Eq. 1 and exemplar optimization in Eq. 2 are separately performed. Essentially, there is no connection between the two optimizations except that the first optimization provides the second one with an initial solution. This causes a critical problem that the exemplar optimization at testing time may not follow the optimization route learned in the training stage, considering that the training-time objective function \mathcal{L}_{train} is different from the exemplar optimization function \mathcal{L}_{expl} , where the former contains 3D SMPL loss while the latter does not.

To solve the above problem and establish connection between the two optimizations, we propose to integrate the exemplar optimization into the training procedure, as shown in Figure 2. Specifically, at each training iteration, we first perform exemplar optimization to update the parameters of network specific to each exemplar, then we perform an actual parameter update by optimizing the training objective. This process is formally formulated as:

$$\mathbf{w}_{opt}^* = \arg \min_{\mathbf{w}} \sum_{i=1}^N \mathcal{L}_{train}(f_{\mathbf{w}'}(\mathbf{I}_i), \hat{\Theta}_i, \hat{\mathbf{J}}_i), \quad (3)$$

where,

$$\mathbf{w}'_i = \mathbf{w} - \alpha \nabla_{\mathbf{w}} \mathcal{L}_{expl}(f_{\mathbf{w}}(\mathbf{I}_i), \hat{\mathbf{J}}_i). \quad (4)$$

The difference between Eq. 3 and Eq. 1 is in the parameters of f to be optimized. Instead of directly optimizing the current parameters \mathbf{w} of f using the training objective \mathcal{L}_{train} , we first perform one step of exemplar optimization using Eq. 4 on each exemplar \mathbf{I}_i to obtain network parameters \mathbf{w}'_i specific to that exemplar. Then, $\{\mathbf{w}'_i | i \in [1, N]\}$

over all training exemplars are in turn used in Eq. 3 to evaluate the training objective. In Eq. 4, α is the learning rate of the exemplar optimization. We perform one step exemplar optimization at each training iteration mainly for saving training time, but this does not prevent us from using more exemplar optimization steps at testing time (we will give more interpretations in Section 4.4).

Remark 1. The benefit of the new formulation in Eq. 3 and 4 is that we can use the training objective to control the behavior of the exemplar optimization. If the exemplar optimization runs in a wrong direction, the following training objective will penalize it and correct the parameter updating direction. After training on the whole training dataset, the exemplar optimization learns to adapt itself to take the optimal behavior to each training exemplar. This endows the exemplar optimization with generalibility, helping alleviate the over-/under-fitting problem at testing time.

3.3. Unifying Training and Exemplar Optimization Objectives with Dual Networks

There are ground-truth human meshes at training time while not at testing time. The training loss \mathcal{L}_{train} can compare the generated mesh with the GT mesh, while \mathcal{L}_{expl} cannot. As mentioned, this is one of the reasons causing the exemplar optimization of EFT [21] to produce inferior results. We have integrated the exemplar optimization into the training procedure to mitigate the gap between the two optimizations. However, the difference in loss functions may hamper the network from learning a shared optimization space for both the objectives. More specifically, since both the exemplar and training optimizations update parameters of the same network, the difference between the two optimization objectives yields different gradient descent directions, causing conflicts that potentially reduce the efficiency of training (see ablation studies in Section 4.4).

To make the exemplar optimization more compatible with the training objective, we propose a method that unifies the training and exemplar optimization objectives by introducing an auxiliary regression network f_u parameterized by \mathbf{u} which is trained together with our main network:

$$\mathbf{w}_{opt}^*, \mathbf{u}_{opt} = \arg \min_{\mathbf{w}, \mathbf{u}} \sum_{i=1}^N (\mathcal{L}_{train}(f_{\mathbf{w}'_i}(\mathbf{I}_i), \hat{\Theta}_i, \hat{\mathbf{J}}_i) + \mathcal{L}_{train}(f_{\mathbf{u}}(\mathbf{I}_i), \hat{\Theta}_i^u, \hat{\mathbf{J}}_i)). \quad (5)$$

The above equation is a combination of Eq. 1 and Eq. 3, with Eq. 1 applied to the auxiliary network f_u , and Eq. 3 applied to the main network f_w . We use f_u to generate a pseudo label $\hat{\Theta}_i^u$ for every training image \mathbf{I}_i , i.e., $\hat{\Theta}_i^u = f_u(\mathbf{I}_i)$, and use the pseudo label to supervise the gradient descent in the exemplar optimization:

$$\mathbf{w}'_i = \mathbf{w} - \alpha \nabla_{\mathbf{w}} \mathcal{L}_{expl}(f_{\mathbf{w}}(\mathbf{I}_i), \hat{\Theta}_i^u, \hat{\mathbf{J}}_i). \quad (6)$$

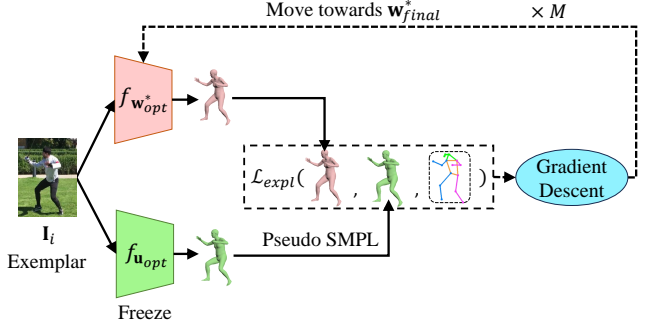


Figure 3. **Inference with dual networks.** We freeze $f_{u_{opt}}$ and use it to compute pseudo GT mesh with which we compute \mathcal{L}_{expl} and use Eq. 6 to update parameters of f_w from \mathbf{w}_{opt}^* to \mathbf{w}_{final}^* iteratively by at most M times.

Please compare between this equation and Eq. 4. The difference is that there is an additional input $\hat{\Theta}_i^u$ to \mathcal{L}_{expl} in the above equation, and note that this new form of \mathcal{L}_{expl} is identical to the form of \mathcal{L}_{train} .

Remark 2. There is a risk that the quality of supervision provided by the auxiliary network is inferior to that of the ground truths. However, since the whole training is supervised under the ground truths, the auxiliary outputs can be viewed as intermediate variables in the framework, which can be trained with other variables together to yield the optimal behavior of the whole system.

3.4. Loss Functions

In this section, we elaborate the loss functions \mathcal{L}_{train} and \mathcal{L}_{expl} . Before defining these losses, we first denote $M(\Theta)$ the 3D vertices of the SMPL human mesh, and $X(\Theta)$ the 3D joints of the human mesh, following the terminology in [22]. \mathcal{L}_{train} is defined as:

$$\mathcal{L}_{train} = \lambda_{2D} \mathcal{L}_{2D} + \lambda_{3D} \mathcal{L}_{3D} + \lambda_{vert} \mathcal{L}_{vert} + \lambda_{SMPL} \mathcal{L}_{SMPL}, \quad (7)$$

with

$$\begin{aligned} \mathcal{L}_{2D} &= \|\pi(X(\Theta)) - \hat{\mathbf{J}}\|_2^2, \\ \mathcal{L}_{3D} &= \|X(\Theta) - X(\hat{\Theta})\|_2^2, \\ \mathcal{L}_{vert} &= \|M(\Theta) - M(\hat{\Theta})\|_2^2, \\ \mathcal{L}_{SMPL} &= \|\Theta - \hat{\Theta}\|_2^2. \end{aligned} \quad (8)$$

In the above equations, $\hat{\Theta}$ and $\hat{\mathbf{J}}$ are GT mesh and joints, Θ represents the generated mesh, and π is the estimated camera. \mathcal{L}_{expl} has the same form as \mathcal{L}_{train} with $\hat{\Theta}$ replaced by the pseudo ground truth $\hat{\Theta}^u$. Note that our loss functions do not include regularization terms as in EFT [21], as our method enforces the regularization implicitly.

3.5. Inference with Dual Networks

Figure 3 shows our new exemplar optimization scheme at testing time. For each test sample \mathbf{I}_i , at our hand are two networks f_w and f_u with $\mathbf{w} = \mathbf{w}_{opt}^*$ and $\mathbf{u} = \mathbf{u}_{opt}$, respectively.

We freeze the parameters of the auxiliary network, and use it to compute the pseudo ground-truth human mesh for the test image \mathbf{I}_i . Then, under the supervision of the pseudo mesh, we compute \mathcal{L}_{expl} and use Eq. 6 to iteratively update the parameters \mathbf{w} of f from \mathbf{w}_{opt}^* to \mathbf{w}_{final}^* . We run at most $M = 14$ iterations, and automatically stop the iteration if losses of two consecutive iterations are close enough. We finally use $f_{\mathbf{w}_{final}^*}$ to estimate human mesh for image \mathbf{I}_i .

3.6. Implementation Details

We implement the main network $f_{\mathbf{w}}$ and auxiliary network $f_{\mathbf{u}}$ with the same network architecture but different parameters. Theoretically, any end-to-end HMR network can be used as f , and we use the method of HMR [22] and CLIFF [32] due to their simplicity. The two methods and many other approaches [7, 8, 25, 33, 55, 56, 60, 61] adopt ResNet-50 [17] or HRNet-W48 [48] to extract features from the input image, and estimate human mesh based on the features. We provide our results of both kinds of backbones.

We implement our method in PyTorch using the Adam optimizer [24] with $\beta_1 = 0.9$ and $\beta_2 = 0.999$. The batchsize for ResNet backbone is 40, and for HRNet backbone is 30. The number of training epochs for ResNet backbone is 65, and for HRNet backbone is 25. The learning rate α used in the exemplar optimization is $1e-5$, and the learning rate for the training optimization is $1e-4$. We set λ_{2D} , λ_{3D} , λ_{vert} , λ_{SMPL} in Eq. 8 to 5.0, 5.0, 0.5, 1.0 (for SMPL pose), 0.001 (for SMPL shape), respectively. Our method takes roughly 3 days training on a single NVIDIA RTX3090 GPU.

4. Experiments

4.1. Datasets

Following previous work [25, 32, 62], we employ the following datasets in our experiments: (1) **Human3.6M** [18], an indoor dataset with precise GT human mesh and 2D joints captured through MoCap devices. (2) **MPI-INF-3DHP** [37], another widely used indoor dataset whose GT human meshes are obtained through multi-view reconstruction. (3) **COCO** [34] and (4) **MPII** [1], two in-the-wild outdoor datasets with human annotated 2D joints for which we use the pseudo GT mesh provided by [32]. (5) **3DPW** [51], a challenging in-the-wild dataset providing accurate human mesh fitted from IMU sensor data.

4.2. Training, Testing and Metrics

Following prior arts [4, 8, 33, 55], we first train our method on a mixture of four datasets, including Human3.6M [18], MPI-INF-3DHP [37], COCO [34], and MPII [1], and then test our method on the test dataset of Human3.6M [18]. After that, we further fine-tune our model for 5 epochs by introducing the training dataset of 3DPW [51], and then evaluate our method on the test dataset of 3DPW [51]. We

Method	3DPW			Human3.6M		
	MPJPE	PA-MPJPE	PVE	MPJPE	PA-MPJPE	
Regression-based	HMR [22]’18	130.0	81.3	-	-	56.8
	PARE [25]’21	79.1	46.4	94.2	-	-
	ROMP [49]’21	76.7	47.3	93.4	-	-
	PyMAF [60]’21	92.8	58.9	110.1	57.7	40.5
	METRO [33]’21	77.1	47.9	88.2	51.2	34.5
	FastMETRO [8]’22	73.5	44.6	84.1	52.2	33.7
	CLIFF [32]’22	69.0	43.0	81.2	47.1	32.7
	LearnSample [55]’22	70.5	43.3	82.7	45.9	33.5
	ProPose [11]’23	68.3	40.6	79.4	45.7	29.1
	POTTER [62]’23	75.0	44.8	87.4	56.5	35.1
	VirtualMarker [36]’23	67.5	41.3	77.9	47.3	32.0
	DeFormer [56]’23	72.9	44.3	82.6	44.8	31.6
BoPR [7]’23	65.4	42.5	80.8	-	-	
Optimization-based	LearnedGD [47]’20	-	55.9	-	-	56.4
	HUND [58]’21	81.4	57.5	-	69.5	52.6
	SPIN [27]’21	96.9	59.2	116.4	62.5	41.1
	EFT [21]’21	85.1	52.2	98.7	63.2	43.8
	HybriK [30]’21	74.1	45.0	86.5	55.4	33.6
	ReFit [53]’23	65.8	41.0	-	48.4	32.2
	NIKI [31]’23	71.3	40.6	86.6	-	-
	PLIKS [45]’23	66.9	42.8	82.6	49.3	34.7
	Ours _{CLIFF} † (HR-W48)	62.9	39.7	80.1	43.9	30.3
	Ours _{CLIFF} * (HR-W48)	57.8	35.3	74.4	39.4	27.5

Table 1. **Quantitative comparison between our method and state-of-the-art methods** on 3DPW [51] and Human3.6M [18]. “†”: using poses detected by OpenPose [6], “*”: using GT 2D poses.

use **MPJPE** (Mean Per Joint Position Error), **PA-MPJPE** (Procrustes-aligned MPJPE), **PVE** (Mean Per-vertex Error) as the metrics to evaluate our method.

4.3. Comparison with Previous Approaches

Quantitative results. We present performance comparison with SOTA methods in Table 1, including regression-based approaches [7, 8, 11, 22, 25, 32, 33, 36, 49, 55, 56, 60, 62] and optimization-based approaches [21, 27, 30, 31, 45, 47, 53, 58]. For all the compared approaches, we report the best results their papers provide. For our method, we adopt CLIFF [32] as the regression network and HRNet-W48 as the backbone network. Since our method needs 2D joints for exemplar optimization, we report results using both GT joints (denoted by \star) or joints estimated by OpenPose [6] (denoted by \dagger).

Please see “Ours_{CLIFF}† (HR-W48)” in Table 1. It is fair to compare this variant of our method with previous SOTA approaches since most of them also use HRNet-W48 as the backbone. This variant of our method uses 2D joints detected by OpenPose instead of the GT joints for the exemplar optimization. As seen, our method outperforms previous approaches significantly. Among the compared approaches,

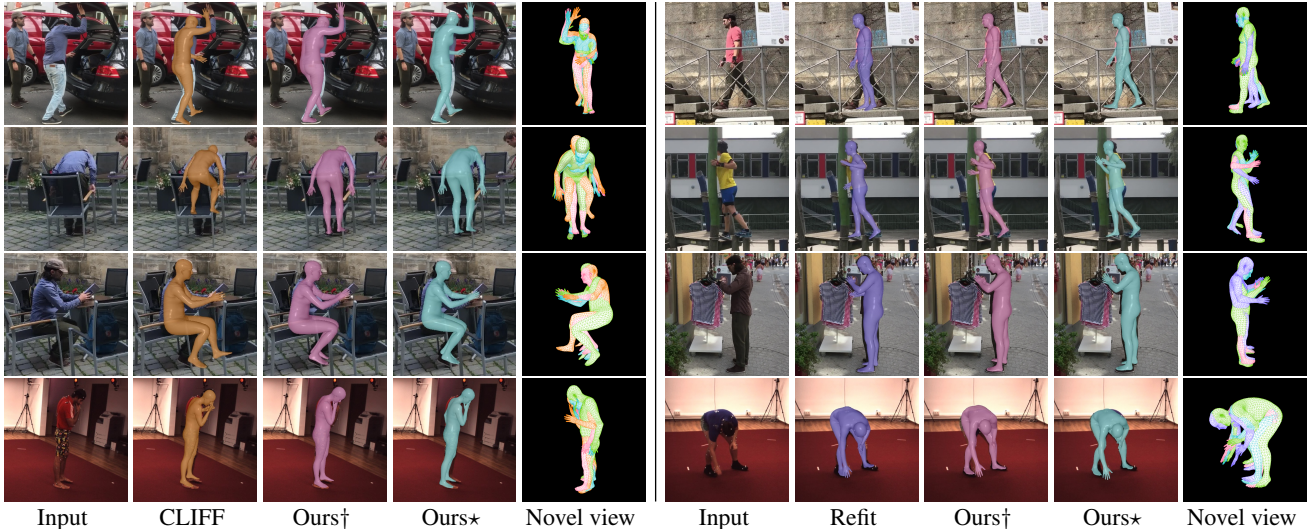


Figure 4. **Qualitative comparison with SOTA methods.** We show results produced by CLIFF [32], ReFit [53], and our method (\dagger : OpenPose, \star : GT pose). All the three methods use HRNet-W48 as the backbone. In the novel views, green represents the ground truth, orange represents CLIFF, purple represents ReFit, pink and blue represent the two variants of our method, respectively.

Method	3DPW			Human3.6M	
	MPJPE	PA-MPJPE	PVE	MPJPE	PA-MPJPE
Ours _{HMR} \dagger (Res-50)	73.3	44.3	90.3	55.8	36.4
Ours _{HMR} \star (Res-50)	68.9	39.6	85.5	53.7	33.8
Ours _{CLIFF} \dagger (Res-50)	66.0	42.1	83.6	46.9	33.1
Ours _{CLIFF} \star (Res-50)	60.9	37.7	77.4	43.1	30.2
Ours _{CLIFF} \dagger (HR-W48)	62.9	39.7	80.1	43.9	30.3
Ours _{CLIFF} \star (HR-W48)	57.8	35.3	74.4	39.4	27.5

Table 2. **Ablation on regression network and source of 2D joints.** The tested regression models include HMR [22] and CLIFF [32]. We test on 2D joints by OpenPose \dagger and GT \star .

VirtualMarker [36] additionally takes advantage of MoCap markers, Metro [33] and DeFormer [56] adopt sophisticated Transformer networks, and NIKI [31] exploits inherent forward and backward kinematics. Our method is free of these techniques, and is only based on the very simple baseline CLIFF [32]. Compared with [32], we improve it from 69.0 to 62.9 taking MPJPE of 3DPW as an example, which is a large margin. Finally, if using GT joints for the exemplar optimization, our method can further improve all the metrics by about 3 to 6mm on both testing datasets.

Qualitative results. We show qualitative comparison with CLIFF [32] and Refit [53] in Fig 4. For these samples, our method estimates faithful human poses and meshes which are better than those of the compared approaches. Considering the absence of ground truth 2D joints in real-world scenarios, we also present results based on the 2D joints estimated by OpenPose [6], which are competitive too. More results are presented in the supplementary material.

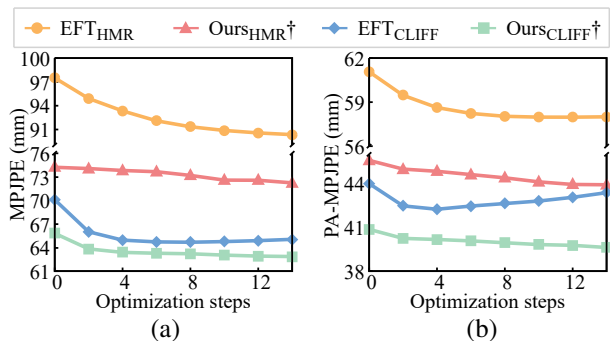


Figure 5. **Influence of optimization steps during inference.** Our method outperforms EFT when using the same regression model. As optimization proceeds, our results continuously become better, while those of EFT become better at first and then become worse.

4.4. Ablation study

Effect of Regression Model. The effectiveness of the adopted regression model essentially influences the effectiveness of our method. In Table 2, we show the results of using HMR [22] and CLIFF [32] as the regression model in our method. Since CLIFF is a stronger baseline than HMR, our method based on CLIFF performs better than that based on HMR. Similarly, since HRNet-W48 is known being better than ResNet-50, our method with HRNet as the backbone outperforms the counterparts taking ResNet as backbone.

Effect of 2D Joints. Since our method needs 2D joints as the supervision at testing time, it is interesting to see how the quality of the 2D joints affects the effectiveness of our method. We test 2D joints detected by OpenPose [6] and

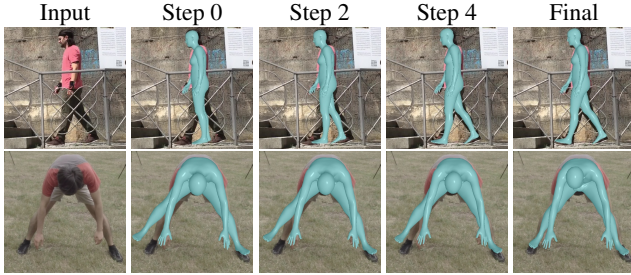


Figure 6. **Stepwise visualization.** From left to right, we showcase results after different steps of exemplar optimization during testing.

Integrating Expl. Opt.	Auxiliary Net	MPJPE ↓	PA-MPJPE ↓
✗	✗	84.6	54.2
✓	✗	78.5	49.9
✓	✓	76.7	49.5

Table 3. **Ablation study on auxiliary network.** Models are trained on COCO [34] and tested on 3DPW [51]. Expl. Opt. represent exemplar optimization.

also the GT 2D joints. Please refer to Table 2 again. Our method with GT joints consistently outperforms our method using detected joints. This indicates our method can become more effective as 2D pose detectors continue to develop.

Effect of Optimization Steps at Inference Time. At inference time, we perform the exemplar optimization iteratively by at most M times. In Figure 5, we show how the evaluation metrics become as the number of optimization steps increases. As seen, our results consistently become better in terms of both MPJPE and PA-MPJPE. We also show the results of EFT_{HMR} and EFT_{CLIFF} . With the same regression model, our method is better than EFT [21]. The results of EFT become better at the first few optimization steps, but become worse as more optimization steps execute.

Figure 6 shows our estimated meshes after some optimization steps. At the very beginning, the mesh does not fit with the target human. After more steps, the mesh progressively deforms itself to achieve perfect fitting.

Recall we only take one exemplar optimization step in a training iteration. One may expect to finish the exemplar optimization at inference time in just a single step too. However, this is not the case as the learning rate ($\alpha = 1e - 5$) is small. Actually, the training takes many iterations. Similarly, we can also take more than one optimization step at testing time, always based on the refined network of the last step.

Effect of Dual Networks. We introduce an auxiliary network to unify the formulation of exemplar and training optimizations, and hope this can reduce the conflict in training and improve the estimation accuracy. We conduct an ablation study to validate this as shown in Table 3. We train all the models in the ablation study on COCO [34] and test

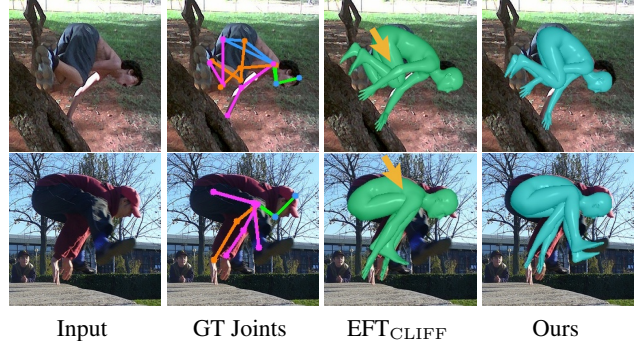


Figure 7. **Out-of-domain adaptation.** Please see the depth of the arms where EFT_{CLIFF} fails to reason, while our method correctly perceive the right configuration.

them on 3DPW [51]. The first row in Table 3 shows results of training with no exemplar (expl.) optimization (opt.) and no auxiliary network, *i.e.*, CLIFF [32]. The second row shows our method without auxiliary network. The third row shows our full method. As shown, the introduction of auxiliary network improves the evaluation results.

Out-of-Domain Adaptation. Exemplar optimization performs specialized post-processing on each test image and has a strong ability to adapt to out-of-domain data. We evaluate the domain adaptation ability of our method and make comparisons with EFT_{CLIFF} on LSP-Extended [20] which is a dataset very different from the training datasets. Our method can handle most of images in this dataset. Figure 7 shows two examples. The persons in the two images take very complex actions. The shadow effect in the images and the similar colors of black pants and shoes make it difficult even for humans to identify the configuration of the 3D meshes. Our method successfully estimates approximately correct meshes with the help of GT poses, while the arms in the results of EFT_{CLIFF} exhibit wrong depth.

Finally, we show more ablations and results in the supplemental material.

5. Conclusion

To conclude, this paper presents a novel training paradigm towards more generalizable exemplar optimization at testing time. We integrate the exemplar optimization into the training procedure, which performs exemplar optimization before running the typical training in each training iteration. We also propose a dual-network architecture to implement this novel training paradigm, aiming at further unifying the target space of the two optimization problems. Extensive experiments and comparisons prove that this new training scheme improves the effectiveness of the exemplar optimization during testing, demonstrating that it successfully learns a prior about how the exemplar optimization should be executed for each exemplar. Ablations show our method can

perform better with stronger regressor baseline or GT 2D poses, and can adapt to out-of-domain challenging test cases.

References

- [1] Mykhaylo Andriluka, Leonid Pishchulin, Peter Gehler, and Bernt Schiele. 2d human pose estimation: New benchmark and state of the art analysis. In *Proceedings of the IEEE Conference on Computer Vision and Pattern Recognition*, pages 3686–3693, 2014. 6
- [2] Antreas Antoniou, Harrison Edwards, and Amos Storkey. How to train your maml. *arXiv preprint arXiv:1810.09502*, 2018. 4
- [3] Alexandru O Bălan and Michael J Black. The naked truth: Estimating body shape under clothing. In *Computer Vision—ECCV 2008: 10th European Conference on Computer Vision, Marseille, France, October 12–18, 2008, Proceedings, Part II 10*, pages 15–29. Springer, 2008. 3
- [4] Michael J Black, Priyanka Patel, Joachim Tesch, and Jinlong Yang. Bedlam: A synthetic dataset of bodies exhibiting detailed lifelike animated motion. In *Proceedings of the IEEE/CVF Conference on Computer Vision and Pattern Recognition*, pages 8726–8737, 2023. 6
- [5] Federica Bogo, Angjoo Kanazawa, Christoph Lassner, Peter Gehler, Javier Romero, and Michael J Black. Keep it smpl: Automatic estimation of 3d human pose and shape from a single image. In *Computer Vision—ECCV 2016: 14th European Conference, Amsterdam, The Netherlands, October 11–14, 2016, Proceedings, Part V 14*, pages 561–578. Springer, 2016. 3
- [6] Zhe Cao, Tomas Simon, Shih-En Wei, and Yaser Sheikh. Realtime multi-person 2d pose estimation using part affinity fields. In *Proceedings of the IEEE conference on computer vision and pattern recognition*, pages 7291–7299, 2017. 1, 4, 6, 7
- [7] Yongkang Cheng, Shaoli Huang, Jifeng Ning, and Ying Shan. Bopr: Body-aware part regressor for human shape and pose estimation. *arXiv preprint arXiv:2303.11675*, 2023. 6
- [8] Junhyeong Cho, Kim Youwang, and Tae-Hyun Oh. Cross-attention of disentangled modalities for 3d human mesh recovery with transformers. In *European Conference on Computer Vision*, pages 342–359. Springer, 2022. 1, 3, 6
- [9] Vasileios Choutas, Federica Bogo, Jingjing Shen, and Julien Valentin. Learning to fit morphable models. In *European Conference on Computer Vision*, pages 160–179. Springer, 2022. 3
- [10] Andrew Davydov, Anastasia Remizova, Victor Constantin, Sina Honari, Mathieu Salzmann, and Pascal Fua. Adversarial parametric pose prior. In *Proceedings of the IEEE/CVF Conference on Computer Vision and Pattern Recognition*, pages 10997–11005, 2022. 3
- [11] Qi Fang, Kang Chen, Yinghui Fan, Qing Shuai, Jiefeng Li, and Weidong Zhang. Learning analytical posterior probability for human mesh recovery. In *Proceedings of the IEEE/CVF Conference on Computer Vision and Pattern Recognition*, pages 8781–8791, 2023. 2, 6
- [12] Chelsea Finn, Pieter Abbeel, and Sergey Levine. Model-agnostic meta-learning for fast adaptation of deep networks. In *International conference on machine learning*, pages 1126–1135. PMLR, 2017. 2, 3
- [13] Michael Fischer and Tobias Ritschel. Metappearance: Meta-learning for visual appearance reproduction. *ACM Transactions on Graphics (TOG)*, 41(6):1–13, 2022. 4
- [14] Peng Guan, Alexander Weiss, Alexandru O Balan, and Michael J Black. Estimating human shape and pose from a single image. In *2009 IEEE 12th International Conference on Computer Vision*, pages 1381–1388. IEEE, 2009. 3
- [15] Shanyan Guan, Jingwei Xu, Yunbo Wang, Bingbing Ni, and Xiaokang Yang. Bilevel online adaptation for out-of-domain human mesh reconstruction. In *Proceedings of the IEEE/CVF Conference on Computer Vision and Pattern Recognition*, pages 10472–10481, 2021. 2, 3
- [16] Nils Hasler, Hanno Ackermann, Bodo Rosenhahn, Thorsten Thormählen, and Hans-Peter Seidel. Multilinear pose and body shape estimation of dressed subjects from image sets. In *2010 IEEE Computer Society Conference on Computer Vision and Pattern Recognition*, pages 1823–1830. IEEE, 2010. 3
- [17] Kaiming He, Xiangyu Zhang, Shaoqing Ren, and Jian Sun. Identity mappings in deep residual networks. In *Computer Vision—ECCV 2016: 14th European Conference, Amsterdam, The Netherlands, October 11–14, 2016, Proceedings, Part IV 14*, pages 630–645. Springer, 2016. 2, 6
- [18] Catalin Ionescu, Dragos Papava, Vlad Olaru, and Cristian Sminchisescu. Human3.6m: Large scale datasets and predictive methods for 3d human sensing in natural environments. *IEEE transactions on pattern analysis and machine intelligence*, 36(7):1325–1339, 2013. 6
- [19] Bangrui Jiang, Zhenhua Guo, and Yujie Yang. Meta-auxiliary network for 3d gan inversion. *arXiv preprint arXiv:2305.10884*, 2023. 4
- [20] Sam Johnson and Mark Everingham. Learning effective human pose estimation from inaccurate annotation. In *CVPR 2011*, pages 1465–1472. IEEE, 2011. 8
- [21] Hanbyul Joo, Natalia Neverova, and Andrea Vedaldi. Exemplar fine-tuning for 3d human model fitting towards in-the-wild 3d human pose estimation. In *2021 International Conference on 3D Vision (3DV)*, pages 42–52. IEEE, 2021. 1, 2, 3, 4, 5, 6, 8
- [22] Angjoo Kanazawa, Michael J Black, David W Jacobs, and Jitendra Malik. End-to-end recovery of human shape and pose. In *Proceedings of the IEEE conference on computer vision and pattern recognition*, pages 7122–7131, 2018. 1, 2, 5, 6, 7
- [23] Mira Kim, Youngjo Min, Jiwon Kim, and Seungryong Kim. Meta-learned initialization for 3d human recovery. In *2022 IEEE International Conference on Image Processing (ICIP)*, pages 4238–4242. IEEE, 2022. 4
- [24] D Kinga, Jimmy Ba Adam, et al. A method for stochastic optimization. In *International conference on learning representations (ICLR)*, page 6. San Diego, California, 2015. 6
- [25] Muhammed Kocabas, Chun-Hao P Huang, Otmar Hilliges, and Michael J Black. Pare: Part attention regressor for 3d human body estimation. In *Proceedings of the IEEE/CVF International Conference on Computer Vision*, pages 11127–11137, 2021. 2, 6

- [26] Muhammed Kocabas, Chun-Hao P Huang, Joachim Tesch, Lea Müller, Otmar Hilliges, and Michael J Black. Spec: Seeing people in the wild with an estimated camera. In *Proceedings of the IEEE/CVF International Conference on Computer Vision*, pages 11035–11045, 2021. 2
- [27] Nikos Kolotouros, Georgios Pavlakos, Michael J Black, and Kostas Daniilidis. Learning to reconstruct 3d human pose and shape via model-fitting in the loop. In *Proceedings of the IEEE/CVF international conference on computer vision*, pages 2252–2261, 2019. 3, 6
- [28] Nikos Kolotouros, Georgios Pavlakos, Dinesh Jayaraman, and Kostas Daniilidis. Probabilistic modeling for human mesh recovery. In *Proceedings of the IEEE/CVF international conference on computer vision*, pages 11605–11614, 2021. 3
- [29] Christoph Lassner, Javier Romero, Martin Kiefel, Federica Bogo, Michael J Black, and Peter V Gehler. Unite the people: Closing the loop between 3d and 2d human representations. In *Proceedings of the IEEE conference on computer vision and pattern recognition*, pages 6050–6059, 2017. 3
- [30] Jiefeng Li, Chao Xu, Zhicun Chen, Siyuan Bian, Lixin Yang, and Cewu Lu. Hybrik: A hybrid analytical-neural inverse kinematics solution for 3d human pose and shape estimation. In *Proceedings of the IEEE/CVF conference on computer vision and pattern recognition*, pages 3383–3393, 2021. 3, 6
- [31] Jiefeng Li, Siyuan Bian, Qi Liu, Jiasheng Tang, Fan Wang, and Cewu Lu. Niki: Neural inverse kinematics with invertible neural networks for 3d human pose and shape estimation. In *Proceedings of the IEEE/CVF Conference on Computer Vision and Pattern Recognition*, pages 12933–12942, 2023. 3, 6, 7
- [32] Zhihao Li, Jianzhuang Liu, Zhensong Zhang, Songcen Xu, and Youliang Yan. Cliff: Carrying location information in full frames into human pose and shape estimation. In *European Conference on Computer Vision*, pages 590–606. Springer, 2022. 1, 2, 6, 7, 8
- [33] Kevin Lin, Lijuan Wang, and Zicheng Liu. End-to-end human pose and mesh reconstruction with transformers. In *Proceedings of the IEEE/CVF conference on computer vision and pattern recognition*, pages 1954–1963, 2021. 1, 2, 6, 7
- [34] Tsung-Yi Lin, Michael Maire, Serge Belongie, James Hays, Pietro Perona, Deva Ramanan, Piotr Dollár, and C Lawrence Zitnick. Microsoft coco: Common objects in context. In *Computer Vision—ECCV 2014: 13th European Conference, Zurich, Switzerland, September 6–12, 2014, Proceedings, Part V 13*, pages 740–755. Springer, 2014. 6, 8
- [35] Matthew Loper, Naureen Mahmood, Javier Romero, Gerard Pons-Moll, and Michael J Black. Smpl: A skinned multi-person linear model. *ACM Transactions on Graphics*, 34(6), 2015. 1, 2, 4
- [36] Xiaoxuan Ma, Jiajun Su, Chunyu Wang, Wentao Zhu, and Yizhou Wang. 3d human mesh estimation from virtual markers. In *Proceedings of the IEEE/CVF Conference on Computer Vision and Pattern Recognition*, pages 534–543, 2023. 6, 7
- [37] Dushyant Mehta, Helge Rhodin, Dan Casas, Pascal Fua, Oleksandr Sotnychenko, Weipeng Xu, and Christian Theobalt. Monocular 3d human pose estimation in the wild using improved cnn supervision. In *2017 international conference on 3D vision (3DV)*, pages 506–516. IEEE, 2017. 6
- [38] Gyeongsik Moon, Hongsuk Choi, and Kyoung Mu Lee. Accurate 3d hand pose estimation for whole-body 3d human mesh estimation. In *Proceedings of the IEEE/CVF Conference on Computer Vision and Pattern Recognition*, pages 2308–2317, 2022. 2
- [39] Hyeongjin Nam, Daniel Sungho Jung, Yeonguk Oh, and Kyoung Mu Lee. Cyclic test-time adaptation on monocular video for 3d human mesh reconstruction. In *Proceedings of the IEEE/CVF International Conference on Computer Vision*, pages 14829–14839, 2023. 3
- [40] Alex Nichol, Joshua Achiam, and John Schulman. On first-order meta-learning algorithms. *arXiv preprint arXiv:1803.02999*, 2018. 4
- [41] Mohamed Omran, Christoph Lassner, Gerard Pons-Moll, Peter Gehler, and Bernt Schiele. Neural body fitting: Unifying deep learning and model based human pose and shape estimation. In *2018 international conference on 3D vision (3DV)*, pages 484–494. IEEE, 2018. 2
- [42] Georgios Pavlakos, Luyang Zhu, Xiaowei Zhou, and Kostas Daniilidis. Learning to estimate 3d human pose and shape from a single color image. In *Proceedings of the IEEE conference on computer vision and pattern recognition*, pages 459–468, 2018. 2
- [43] Georgios Pavlakos, Vasileios Choutas, Nima Ghorbani, Timo Bolkart, Ahmed AA Osman, Dimitrios Tzionas, and Michael J Black. Expressive body capture: 3d hands, face, and body from a single image. In *Proceedings of the IEEE/CVF conference on computer vision and pattern recognition*, pages 10975–10985, 2019. 3
- [44] Aravind Rajeswaran, Chelsea Finn, Sham M Kakade, and Sergey Levine. Meta-learning with implicit gradients. *Advances in neural information processing systems*, 32, 2019. 4
- [45] Karthik Shetty, Annette Birkhold, Srikrishna Jaganathan, Norbert Strobel, Markus Kowarschik, Andreas Maier, and Bernhard Egger. Pliks: A pseudo-linear inverse kinematic solver for 3d human body estimation. In *Proceedings of the IEEE/CVF Conference on Computer Vision and Pattern Recognition*, pages 574–584, 2023. 3, 6
- [46] Leonid Sigal, Alexandru Balan, and Michael Black. Combined discriminative and generative articulated pose and non-rigid shape estimation. *Advances in neural information processing systems*, 20, 2007. 3
- [47] Jie Song, Xu Chen, and Otmar Hilliges. Human body model fitting by learned gradient descent. In *European Conference on Computer Vision*, pages 744–760. Springer, 2020. 3, 6
- [48] Ke Sun, Bin Xiao, Dong Liu, and Jingdong Wang. Deep high-resolution representation learning for human pose estimation. In *Proceedings of the IEEE/CVF conference on computer vision and pattern recognition*, pages 5693–5703, 2019. 6
- [49] Yu Sun, Qian Bao, Wu Liu, Yili Fu, Michael J Black, and Tao Mei. Monocular, one-stage, regression of multiple 3d people. In *Proceedings of the IEEE/CVF international conference on computer vision*, pages 11179–11188, 2021. 6

- [50] Vince Tan, Ignas Budvytis, and Roberto Cipolla. Indirect deep structured learning for 3d human body shape and pose prediction. In *BMVC*, page 6, 2017. 2
- [51] Timo Von Marcard, Roberto Henschel, Michael J Black, Bodo Rosenhahn, and Gerard Pons-Moll. Recovering accurate 3d human pose in the wild using imus and a moving camera. In *Proceedings of the European conference on computer vision (ECCV)*, pages 601–617, 2018. 6, 8
- [52] Wenjia Wang, Yongtao Ge, Haiyi Mei, Zhongang Cai, Qingping Sun, Yanjun Wang, Chunhua Shen, Lei Yang, and Taku Komura. Zolly: Zoom focal length correctly for perspective-distorted human mesh reconstruction. *arXiv preprint arXiv:2303.13796*, 2023. 1, 2
- [53] Yufu Wang and Kostas Daniilidis. Refit: Recurrent fitting network for 3d human recovery. *arXiv preprint arXiv:2308.11184*, 2023. 6, 7
- [54] Xiangyu Xu, Hao Chen, Francesc Moreno-Noguer, László A Jeni, and Fernando De la Torre. 3d human shape and pose from a single low-resolution image with self-supervised learning. In *Computer Vision—ECCV 2020: 16th European Conference, Glasgow, UK, August 23–28, 2020, Proceedings, Part IX 16*, pages 284–300. Springer, 2020. 2
- [55] Youze Xue, Jiansheng Chen, Yudong Zhang, Cheng Yu, Huimin Ma, and Hongbing Ma. 3d human mesh reconstruction by learning to sample joint adaptive tokens for transformers. In *Proceedings of the 30th ACM International Conference on Multimedia*, pages 6765–6773, 2022. 1, 2, 6
- [56] Yusuke Yoshiyasu. Deformable mesh transformer for 3d human mesh recovery. In *Proceedings of the IEEE/CVF Conference on Computer Vision and Pattern Recognition*, pages 17006–17015, 2023. 1, 3, 6, 7
- [57] Andrei Zanfir, Eduard Gabriel Bazavan, Hongyi Xu, William T Freeman, Rahul Sukthankar, and Cristian Sminchisescu. Weakly supervised 3d human pose and shape reconstruction with normalizing flows. In *Computer Vision—ECCV 2020: 16th European Conference, Glasgow, UK, August 23–28, 2020, Proceedings, Part VI 16*, pages 465–481. Springer, 2020. 2
- [58] Andrei Zanfir, Eduard Gabriel Bazavan, Mihai Zanfir, William T Freeman, Rahul Sukthankar, and Cristian Sminchisescu. Neural descent for visual 3d human pose and shape. In *Proceedings of the IEEE/CVF Conference on Computer Vision and Pattern Recognition*, pages 14484–14493, 2021. 3, 6
- [59] Bowen Zhang, Chenyang Qi, Pan Zhang, Bo Zhang, Hsiang-Tao Wu, Dong Chen, Qifeng Chen, Yong Wang, and Fang Wen. Metaportrait: Identity-preserving talking head generation with fast personalized adaptation. In *Proceedings of the IEEE/CVF Conference on Computer Vision and Pattern Recognition*, pages 22096–22105, 2023. 4
- [60] Hongwen Zhang, Yating Tian, Xinchu Zhou, Wanli Ouyang, Yebin Liu, Limin Wang, and Zhenan Sun. Pymaf: 3d human pose and shape regression with pyramidal mesh alignment feedback loop. In *Proceedings of the IEEE/CVF International Conference on Computer Vision*, pages 11446–11456, 2021. 2, 3, 6
- [61] Hongwen Zhang, Yating Tian, Yuxiang Zhang, Mengcheng Li, Liang An, Zhenan Sun, and Yebin Liu. Pymaf-x: Towards well-aligned full-body model regression from monocular images. *IEEE Transactions on Pattern Analysis and Machine Intelligence*, 2023. 2, 3, 6
- [62] Ce Zheng, Xianpeng Liu, Guo-Jun Qi, and Chen Chen. Potter: Pooling attention transformer for efficient human mesh recovery. In *Proceedings of the IEEE/CVF Conference on Computer Vision and Pattern Recognition*, pages 1611–1620, 2023. 1, 6
- [63] Shizhe Zhou, Hongbo Fu, Ligang Liu, Daniel Cohen-Or, and Xiaoguang Han. Parametric reshaping of human bodies in images. *ACM transactions on graphics (TOG)*, 29(4):1–10, 2010. 3
- [64] Xilong Zhou and Nima Khademi Kalantari. Look-ahead training with learned reflectance loss for single-image svbrdf estimation. *ACM Transactions on Graphics (TOG)*, 41(6):1–12, 2022. 4